Research Square

Preprints are preliminary reports that have not undergone peer review.
They should not be considered conclusive, used to inform clinical practice,
or referenced by the media as validated information.

Bioprinted aquatic plant-inspired soft machines for underwater environmental sensing

Isabella Fiorello

i.fiorello@imperial.ac.uk

Imperial College London https://orcid.org/0000-0003-2613-9505

Israel Kellersztein

Ben-Gurion University of the Negev

Beatriz Arsuffi

Empa, Swiss Federal Laboratories for Materials Science and Technology

Frederike Klimm

University of Freiburg

Barbara Mazzolai

Italian Institute of Technology https://orcid.org/0000-0003-0722-8350

Thomas Speck

Faculty of Biology, University of Freiburg https://orcid.org/0000-0002-2245-2636

Chiara Daraio

California Institute of Technology https://orcid.org/0000-0001-5296-4440

Article

Keywords:

Posted Date: November 6th, 2026

DOI: https://doi.org/10.21203/rs.3.rs-11412743/v1

License: This work is licensed under a Creative Commons Attribution 4.0 International License.
Read Full License

Additional Declarations: There is **NO** Competing Interest.

Title

Bioprinted aquatic plant-inspired soft machines for underwater environmental sensing

Authors

Isabella Fiorello[1, 2, 3, 4]*, Israel Kellersztein[4, 5], Beatriz Arsuffi[4,6], Frederike Klimm[3], Barbara Mazzolai[7], Thomas Speck[2,3#]*, and Chiara Daraio[4#]*

Affiliations

[1] Department of Life Sciences, Imperial College, London, United Kingdom

[2] Cluster of Excellence *liv*MatS@FIT - Freiburg Center for Interactive Materials and Bioinspired Technologies, University of Freiburg, Germany

[3]Plant Biomechanics Group, University of Freiburg, Freiburg, Germany

[4]Division of Engineering and Applied Science, California Institute of Technology, Pasadena, California

[5]Department of Materials Engineering, Ben-Gurion University of the Negev, Beer-Sheva 84105, Israel

[6]Cellulose and Wood Materials Laboratory, Empa, Swiss Federal Laboratories for Materials Science and Technology, 8600 Dübendorf, Switzerland.

[7]Bioinspired Soft Robotics Laboratory, Istituto Italiano di Tecnologia, Genoa, Italy

#equally contributed

*Corresponding authors: i.fiorello@imperial.ac.uk; thomas.speck@biologie.uni-freiburg.de; daraio@caltech.edu

Abstract

Aquatic plants combine porous, compliant stems with distributed leaves that interact with complex underwater environments, but these design principles remain unexplored in soft robotics. Here we translate the architecture and biomechanics of the submerged macrophyte *Myriophyllum mattogrossense* into bioprinted aquatic plant-inspired soft machines. High-resolution photon-based bioprinting produced wheel-like porous hydrogel stems with approximately 38% lower flexural

rigidity than solid controls (15.6 ± 2.1 versus 25.1 ± 2.8 N mm²), enabling large deformations under external loading. We fabricated leaf-like structures using two cellulose-based hydrogel systems. Sodium alginate-hydroxyethyl cellulose hydrogels containing *Chlamydomonas reinhardtii* showed progressive greening and chlorophyll autofluorescence during culture. Nanocellulose-based poly(N-isopropylacrylamide) hydrogels underwent reversible shape changes in response to temperature and salinity, with curvature increasing 6.5-fold and 4-fold, respectively. Integrating these components produced an artificial aquatic plant-like machine that remained stable underwater while retaining the mechanical and responsive properties of its stem and leaf modules. These results establish aquatic plant architecture as a source of design principles for modular biohybrid soft machines and provide a foundation for underwater environmental sensing. This responsive platform offers a route towards adaptive underwater devices for environmental monitoring, ecological research and future biohybrid robotic applications across diverse, dynamic aquatic ecosystems.

Main text

Introduction

Aquatic ecosystems, including rivers, lakes, oceans, and coastal environments, are experiencing rapid environmental change driven by climate change and human activities[1]. Addressing these challenges requires technologies capable of operating within complex, dynamic, and fragile environments while minimizing ecological disturbance and interacting seamlessly with living ecosystems[2]. In this context, bioinspired soft robotics has emerged as a promising approach for developing compliant machines that can safely interact with real-world unstructured ecosystems[3-7]. Living organisms provide a powerful source of inspiration for such technologies, as they have evolved strategies to operate robustly within heterogeneous and continuously changing environments[8]. Among them, plants have recently attracted growing attention in robotics because of the remarkable adaptations that enable them to thrive across diverse habitats, from terrestrial to aquatic environments[3,9-11]. These characteristics have led to the development of plant-inspired soft robotic machines that translate biological principles such as growth, distributed sensing, and

environmental adaptation into engineered devices[11-15]. When miniaturized, these systems can operate on complex three-dimensional surfaces and within highly constrained environments[16-19]. Plant-inspired soft robotics has predominantly drawn inspiration from terrestrial species, with applications ranging from climbing robots and adaptive manipulators to soil exploration and reforestation technologies[17-20]. Aquatic plants provide an additional distinct design space: their load-bearing axes remain compliant, whereas spatially distributed leaves form extensive interfaces with the surrounding water. This separation between compliant structural support and environmental interaction provides a useful model for soft machines designed to operate in complex underwater environments.

Aquatic plants have evolved specialized morphological and biomechanical traits, including porous tissues, hollow stems and compliant leaf architectures[21]. Species such as *Myriophyllum* spp. and aquatic *Ranunculus* spp. combine structural support with flexibility under hydrodynamic loading[21]. Mimicking the traits of stems and leaves found in aquatic plants provides transferable design principles for constructing soft robotic systems that can remain compliant and responsive underwater.

Recent advances in additive manufacturing and bioprinting have opened new opportunities for fabricating bioinspired soft robotic structures with complex architectures[22,23]. Techniques such as direct-ink writing, bioprinting, stereolithography, and multiphoton polymerization enable the fabrication of microscale structures with controlled geometry, porosity, and mechanical properties, making them particularly suitable for replicating the structural complexity found in biological systems[24,25]. These approaches have been increasingly explored for the development of soft robotic components, functional materials and biohybrid systems, enabling the integration of sensing, actuation, and environmental responsiveness within miniaturized architectures[26].

Here, we present an aquatic plant-inspired biohybrid soft machine fabricated using complementary high-resolution bioprinting approaches. Inspired by the submerged macrophyte *Myriophyllum mattogrossense*, we combine photon-based bioprinting of lightweight porous stem-like architectures

with extrusion bioprinting of compliant leaf-like structures. The stems provide compliant structural support, whereas the leaves incorporate either living microalgae or a multistimuli-responsive hydrogel. Integrating these components produces an artificial aquatic plant-like machine that combines plant-inspired architecture with living and stimulus-responsive functions. This modular approach demonstrates how high-resolution bioprinting can translate the structural and functional features of aquatic plants into responsive underwater soft machines, providing a foundation for future applications in environmental monitoring, underwater exploration and ecological research.

Results

Bioinspired concept

The submerged aquatic plant *Myriophyllum mattogrossense* was selected as the biological model for this study because members of the genus exhibit lightweight porous stems, compliant leaves, and specialized biomechanical adaptations that enable survival under hydrodynamic loading[21]. An overview of the bioinspired concept is provided in **Supplementary Fig. 1**. Plants were cultivated and analyzed under controlled aquatic conditions (**Supplementary Fig. 2, Supplementary Movies 1** and **2**). Morphological analyses of the stems and leaves identified two key biological design principles that guided the development of the artificial system: a slender stem with a wheel-like porous cross-section and finely branched leaves distributed along the plant axis (**Fig. 1a, Supplementary Fig. 3**). These features were translated into distinct structural and functional modules of the artificial system enabling efficient adaptation to complex and dynamic underwater environments[21].

Cross-sectional analyses using optical microscopy, histology, and scanning electron microscopy revealed a central vascular cylinder surrounded by wheel-shaped aerenchyma lacunae, forming a lightweight porous architecture that reduces density while maintaining structural support (**Fig. 1b-d**). Distinct morphological variations were observed along the shoot axis, including apical, middle, and basal stem regions (**Supplementary Fig. 3**), indicating local specialization of the stem architecture. In particular, the geometry of the wheel-like internal structure varied, with changes in

105 the size and distribution of the radial air cavities. This axial variation was characterized in the
106 natural plant but was not directly reproduced in the artificial stem, which mimicked only a short
107 basal stem section.
108 Leaf analyses revealed feather-like pinnate leaves with aligned tissues that support flexibility and
109 passive reconfiguration (**Fig. 1e-g**). Leaf morphology varied along the plant axis, with compact
110 basal leaves transitioning into more elongated and dissected apical structures (**Supplementary Fig.**
111 **4**). Histological analyses further revealed large intercellular spaces in the leave parenchyma
112 (**Supplementary Fig. 5**). These observations motivated the development of compliant, spatially
113 distributed artificial leaf modules.
114 Mechanical characterization in tension and bending was performed on natural *M. mattogrossense*
115 stems using custom-made dedicated setups (**Supplementary Figs. 6 and 9**). Tensile testing
116 revealed comparable structural Young's moduli across the basal, middle, and apical stem regions
117 (31.7 ± 16.4, 22.9 ± 9.0, and 23.4 ± 7.7 MPa, respectively; **Fig. 1l**), with corresponding breaking
118 strains of 7.0 ± 2.7%, 6.2 ± 1.5%, and 8.4 ± 1.8% (Supplementary Fig. 7). Representative stress–
119 strain curves showed the characteristic nonlinear tensile response of the stems (**Fig. 1n** and
120 **Supplementary Fig. 8**; Supplementary Movie 3). Similarly, bending stiffness showed no
121 significant variation along the stem, with values of 3.5 ± 1.8, 3.3 ± 2.8, and 2.8 ± 2.1 N mm² in the
122 basal, middle, and apical regions, respectively (**Fig. 1m** and **Supplementary Fig. 10**). While
123 mechanical properties remained relatively uniform along the stem, both diameter and cross-
124 sectional area decreased at the apical region (**Supplementary Fig. 11**). Together, these results
125 indicate that *M. mattogrossense* maintains broadly comparable effective mechanical properties
126 along the stem despite axial changes in geometry, consistent with previous biomechanical
127 observations in *Myriophyllum* species[21]. The comparable Young's modulus across stem regions
128 further indicates that tissue material properties remain largely constant, suggesting that structural
129 adaptation is achieved primarily through geometric rather than material variation. This principle
130 informed the biomimetic translation of the biological architecture, in which geometric modulation

of a single constituent material was used to generate an artificial stem with a distinct bioinspired geometry as compared to a solid cylinder.

Three-dimensional micro-computed tomography (μCT) further resolved the internal organization of stems and leaves, revealing the continuous porous stem architecture and the spatial arrangement of the leaves along the shoot axis (**Fig. 1h, i**). Additional μCT analyses confirmed these structural features across different plant regions (**Supplementary Fig. 12-15**; **Supplementary Movie 4**). The reconstructed geometry was processed to extract the principal features of the stem cross-section and generate the biomimetic CAD model used for bioprinting. These analyses established the translation from the natural plant to an artificial system comprising a porous stem and distributed leaf-like structures (**Supplementary Fig. 16** and **Supplementary Movies 5-8**).

Bioprinting and characterization of artificial stems

To replicate the structural characteristics of aquatic plant stems, artificial stems were fabricated using photon-based bioprinting of hydrogel-based materials (**Figure 2a**; bioprinting parameters in **Supplementary Table 1**). The light-based bioprinting process using the LUMEN X platform is shown in **Supplementary Movie 9**. Preliminary fabrication optimization demonstrated that shorter stem geometries enabled stable printing fidelity and structural integrity, whereas elongated unsupported architectures resulted in deformation and reduced fabrication accuracy (**Supplementary Fig. 16**). The optimized printing strategy enabled the generation of cylindrical structures with internal architectures inspired by the porous organization observed in natural plant stems.

Optical imaging of the printed constructs confirmed the presence of a well-defined internal structure characterized by radially arranged cavities surrounding a central core (**Fig. 2b**). Longitudinal views revealed aligned microstructures along the printing direction, indicating controlled material deposition and consistent fabrication fidelity (**Fig. 2c**). The printed geometry therefore reproduced the central architectural principle extracted from the natural stem, i.e. the distribution of material around an internal network of longitudinal cavities.

The mechanical properties of the artificial stems were evaluated using tensile and bending tests. Under uniaxial tensile loading, the constructs exhibited an approximately linear stress-strain response up to failure (**Fig. 2d** and **Supplementary Movie 10**). Plant-inspired artificial stems exhibited mean breaking strains of approximately 4.0%, compared with approximately 3.5% for solid control stems, and mean tensile strengths of approximately 0.55 and 0.39 MPa, respectively (**Fig. 2e, f**). These measurements indicate similar tensile behavior at the tested sample sizes, whereas the influence of the internal architecture was more apparent under bending. The tensile-test setup is shown in **Fig. 2g**.

Three-point bending tests were used to assess structural compliance. The resulting force-displacement curves showed stable deformation under bending loads (**Fig. 2h**). Compared with solid controls printed using the same material and external geometry, the porous stems exhibited an approximately 38% reduction in flexural rigidity, from 25.1 ± 2.8 to 15.6 ± 2.1 N mm² (**Fig. 2i**). Introducing the porous internal architecture while maintaining the same outer diameter and hydrogel composition reduced the amount of load-bearing material and the bending stiffness. The corresponding apparent flexural moduli are shown in **Fig. 2l**. The porous stems accommodated large bending deformations under applied loading (**Fig. 2m**), demonstrating how plant-derived geometry can tune the compliance of bioprinted supports.

Bioprinting and characterization of artificial leaves

Artificial leaf-like structures inspired by the distributed leaves of aquatic plants were fabricated by direct ink writing (DIW). These structures were designed to introduce complementary functionalities into the biohybrid platform by two distinct cellulose-based hydrogel systems: a living hydrogel producing an optical biological output and a responsive hydrogel converting changes in the aqueous environment into mechanical deformation.

First, leaf-like structures composed of sodium alginate-hydroxyethyl cellulose hydrogels were used to encapsulate the microalga *Chlamydomonas reinhardtii*. The preparation of the hydrogel-algae bioink, the extrusion-based bioprinting workflow and the optimized printing parameters are shown

in **Supplementary Figs. 17** and **18** and **Supplementary Table 2**. The bioprinting process is presented in **Supplementary Movie 11**. Optical imaging showed progressive greening of the printed constructs during culture (**Fig. 3a-c**). Confocal microscopy and three-dimensional reconstructions further revealed chlorophyll autofluorescence distributed throughout the hydrogel network (**Fig. 3d-i**). Together, these observations demonstrate the persistence and spatial distribution of a microalgal optical signal within the printed leaf-like structures. The microalgae-containing leaves therefore provide living optical interfaces that could be calibrated for biologically mediated sensing. Because microalgae respond to environmental variables including temperature, pH, nutrient availability and pollutants, these structures offer a platform for developing living sensors for aquatic environments[27,28].

A second class of artificial leaves was fabricated using a responsive PNIPAM/nanocellulose hydrogel (**Fig. 4**). Direct ink writing is well suited to 4D printing because it enables the fabrication of material architectures that undergo programmed shape changes in response to external stimuli[29]. The preparation of the hydrogel, fabrication process, optimized printing parameters, and final printed structures are described in **Supplementary Fig. 19** and **Supplementary Table 2**, whereas the printing process is shown in **Supplementary Movie 12**. Above the lower critical solution temperature (LCST) of PNIPAM (32 °C), the printed leaves underwent pronounced shrinking (**Fig. 4a**). Crossing the LCST triggered a rapid reduction in projected surface area from 100% to approximately 78%, accompanied by an increase in bending curvature from ~0.08 to ~0.67 cm^{-1} (**Fig. 4b,d** and **Supplementary Figs. 20** and **21**). Representative surface area and bending curvature changes under different temperature and solution conditions are shown in **Supplementary Movies 13** and **14**, respectively. Both responses were fully reversible over repeated heating and cooling cycles, demonstrating reproducible thermoresponsive actuation. Similarly, exposure to 6 M NaCl reduced the LCST of PNIPAM and therefore induced a reduction in projected surface area from 100% to approximately 73%, increasing the bending curvature from near-zero values to ~0.40 cm^{-1}

(**Fig. 4c,e**). These experiments demonstrate reversible thermal and salt-responsive actuation of the printed leaves under the applied conditions.

Together, the two leaf systems provide distinct outputs within the same distributed architecture. The microalgae-containing leaves provide a living, optically readable interface, whereas the PNIPAM/nanocellulose leaves convert changes in temperature and salinity into reversible changes in area and curvature. Their integration within a shared plant-inspired geometry demonstrates the modularity of the bioprinting strategy, providing the foundation for the development of multifunctional biohybrid soft robotic underwater systems.

Proof-of-concept **integrated demonstrator**

The artificial stems and leaf-like structures were assembled to produce an artificial aquatic plant-like machine. The resulting systems reproduce the general architecture of submerged aquatic plants, consisting of a compliant central stem supporting distributed functional leaf-like structures (**Fig. 5a, b**). Representative underwater visualizations of assembled artificial aquatic plants with stems and hydrogel leaves of different sizes are shown in **Supplementary Movies 15-18**.

The fabrication and integration workflow are illustrated in **Supplementary Fig. 22**, including stem fabrication, UV curing, attachment of the hydrogel leaf-like structures, and the final assembled devices. The modular fabrication approach enabled leaf-like hydrogels with different sizes, geometries, and material compositions to be readily combined with the printed stems, generating diverse plant-inspired architectures (**Supplementary Figs. 23** and **24**). Multiple leaf modules were further integrated along a single stem to produce multi-section artificial aquatic plants with distributed leaf-like structures (**Supplementary Fig. 25**). The compliant hydrogel leaves exhibited passive reconfiguration underwater that depended on their morphology and material composition, enabling the assembled structures to adapt their overall configuration in a manner analogous to submerged aquatic vegetation. Manual underwater handling demonstrated that the assembled structures remained mechanically stable and compliant under repeated bending and manipulation, without visible structural damage or leaf detachment (**Fig. 5c, d**).

To demonstrate system-level functionality, the assembled biohybrid plants were deployed in water-filled containers under different environmental conditions (**Fig. 5e, Supplementary Fig. 26**). The integrated structures remained mechanically stable while exhibiting passive shape reconfiguration in response to external stimuli. Representative underwater demonstrations of the temperature- and salinity-responsive systems are shown in **Supplementary Movies 19** and **20**.

These proof-of-concept experiments demonstrate that independently fabricated structural and functional modules can be assembled into an integrated aquatic plant-like machine while retaining their respective mechanical and responsive properties.

Conclusions

We translated structural and functional principles from the submerged macrophyte *Myriophyllum mattogrossense* into bioprinted aquatic plant-inspired soft machines. The design separates mechanical support from environmental interaction: a radially porous stem provides structural compliance, whereas distributed hydrogel leaves provide living optical or mechanically responsive interfaces.

The printed stems reproduced the wheel-like architecture of natural plant tissues. Compared with fully filled controls, the porous geometry reduced flexural rigidity by approximately 38% and enabled large bending deformations. Microalgae-containing leaves retained a spatially distributed chlorophyll-autofluorescence signal during culture, whereas PNIPAM/nanocellulose leaves reversibly converted changes in temperature and salinity into changes in projected area and curvature.

Integrating these components produced an artificial aquatic plant-like machine that remained stable underwater while retaining the mechanical and responsive properties of its stem and leaf modules. The system demonstrates how biological architecture, high-resolution bioprinting and functional hydrogels can be combined within a modular underwater platform.

More broadly, this work identifies aquatic plant architecture as a source of design principles for biohybrid soft machines. The modular approach can be extended to other aquatic growth forms,

including partially submerged species such as *Myriophyllum brasiliense* (Supplementary Fig. 27), and provides a foundation for adaptive underwater devices for environmental monitoring, ecological research and biohybrid robotics.

Methods

Plant materials. Specimens of *Myriophyllum mattogrossense* were obtained from a commercial aquatic plant supplier (Flowgrow, Germany). Plants were maintained in a freshwater tank in a greenhouse at a water temperature of approximately 20-25 °C (Botanical Garden, Freiburg, Germany) (**Supplementary Fig. 2a, b**). For observational experiments in a controlled underwater environment, plants were removed from the greenhouse tank and transferred to a laboratory aquarium setup (**Supplementary Fig. 2c, d**). Stem and leaf samples were collected from mature plants and rinsed with deionized water prior to structural and mechanical characterization.

X-ray microcomputed tomography (μCT) investigations. The internal morphology of stems and leaves of *Myriophyllum mattogrossense* was investigated using X-ray microcomputed tomography (μCT). To prepare the samples for μCT analysis, freshly excised plant samples were fixed in 100% methanol for 5 min and subsequently infiltrated with 1% phosphotungstic acid (PTA) in 100% methanol for 3 days to enhance X-ray contrast. To prevent sample deformation during drying, a critical point dryer (Bal-Tec CPD 030, BAL-TEC AG, United States) was used prior to scanning. The samples were then mounted in plastic holders to minimize movement during scanning. Scans were performed using an X-ray microcomputed tomography system (ProCon X-Ray, PXR GmbH, Germany). The scanning parameters included an acceleration voltage of 60 kV, a source current of 100 μA, an exposure time of 0.3 s, and a focal spot size of 8 μm. Projection images were acquired over a full 360° rotation and reconstructed using the system's reconstruction software. The resulting three-dimensional datasets were processed and visualized using VGStudio (Volume Graphics, Germany).

Scanning Electron Microscopy (SEM) investigations. The surface morphology of natural stems and leaves was investigated by scanning electron microscopy (SEM). Freshly excised plant stems

and leaves were chemically fixed in 2.5% (v/v) glutaraldehyde and dehydrated through a graded ethanol series. The samples were subsequently dried by critical point drying (Baltec CPD 030 Critical Point Dryer, USA) to preserve their three-dimensional morphology. All specimens were mounted on aluminium stubs and sputter-coated with a 15 nm gold layer. SEM imaging was performed using a Zeiss EVO scanning electron microscope (Carl Zeiss Microscopy GmbH, Oberkochen, Germany) operated at an accelerating voltage of 5-10 kV.

Digital microscopy investigations. The morphology of the bioprinted stem and leaf-inspired structures was examined using a stereomicroscope (SMZ25, Nikon Corporation, Tokyo, Japan). Natural plant stems and leaves were imaged using a BX61 optical microscope (Olympus Corporation, Tokyo, Japan).

Histology. Histological analyses were performed on natural stems and leaves. Fresh samples were fixed in FAA solution (formaldehyde-acetic acid-ethanol) and dehydrated through a graded isopropanol series consisting of 70%, 90% (2 h), and two successive incubations in 100% isopropanol (30 min and 1 h) at room temperature. Following dehydration, the samples were pre-infiltrated overnight at room temperature in a 1:1 (v/v) mixture of 100% isopropanol and Technovit 7100 base solution (Kulzer GmbH, Wehrheim, Germany). Samples were subsequently infiltrated overnight at 4 °C in Technovit 7100 base solution containing Hardener I (1 g per 100 mL base solution). Polymerization was carried out in embedding molds by adding Hardener II according to the manufacturer's instructions. The embedded samples were sectioned using a rotary microtome to obtain transverse and longitudinal sections of stems and leaves. Sections were stained with Toluidine Blue O and imaged using a BX61 optical microscope (Olympus Corporation, Tokyo, Japan).

Confocal fluorescence microscopy investigations. A confocal microscope (Nikon Ti2-E inverted microscope) was used to visualize microalgae encapsulated within hydrogel matrices. Samples were placed on microscope slides and imaged using a laser scanning confocal microscope equipped with appropriate excitation and emission filters for chlorophyll autofluorescence. Z-stack image series

were acquired to reconstruct the three-dimensional spatial distribution of microalgae within the hydrogel structures.

Bioprinting of artificial stems. Artificial stems were fabricated using high-resolution light-based bioprinting. The plant-inspired stem structures were designed based on the internal architecture observed in natural aquatic plant stems. The stems were printed in two configurations: (i) stems with a porous wheel-like architecture mimicking natural stems, and (ii) fully filled control stems used for mechanical comparison. Three-dimensional (3D) CAD models of the artificial stems were generated and exported as STL files. The models were first processed using slicing software (PrusaSlicer, Prusa Research, Czech Republic). The sliced files were then imported into DNA Studio Illuminate software (Cellink, Sweden) for print preparation and parameter setup. To ensure stable attachment of the printed structures to the build platform, a base substrate (1.5 mm in diameter and 0.8 mm in height) was added to the stem CAD model using DNA Studio Illuminate software. The artificial stems were printed using a digital light processing (DLP) bioprinter (LumenX, Cellink, Sweden) and a biocompatible photosensitive hydrogel bioink composed of polyethylene glycol diacrylate (PEGDA; PEGDA X, Cellink). Printing was performed using a 405 nm UV light source. The layer height was set to 50 μm, with an exposure time of 3 s per layer and a light intensity of 70% (Table 1). To improve adhesion between the substrate and the build platform, the first three layers were exposed for 9 s at 100% light intensity. Immediately after printing, the samples were carefully removed from the build platform and immersed in deionized water overnight to remove uncured resin.

Preparation of microalgae-based SA/HEC bioink. The microalgae-based bioink was prepared using a sodium alginate/hydroxyethyl cellulose (SA/HEC) hydrogel formulation. Briefly, 0.75 g of sodium alginate and 2.25 g of hydroxyethyl cellulose were added to 25 mL of TAP medium, corresponding to final concentrations of 3% (w/v) sodium alginate and 9% (w/v) hydroxyethyl cellulose. The components were mixed until a homogeneous hydrogel precursor was obtained using a mechanical mixer. Separately, 10 mL of *Chlamydomonas reinhardtii* culture were collected and

centrifuged to pellet the cells. The supernatant TAP medium was removed, and the cell pellet was resuspended in fresh TAP medium. The algal suspension was then gently mixed with the SA/HEC hydrogel precursor using a spatula to obtain a homogeneous microalgae-containing bioink. The bioink was transferred into a syringe, centrifuged to remove entrapped air bubbles, and used for extrusion-based bioprinting. After printing, the hydrogel constructs were crosslinked in 0.1 M $CaCl_2$ for 20 min. Excess $CaCl_2$ was removed, and the printed samples were rinsed/immersed in TAP medium. For storage and culture after printing, approximately 10 mL of TAP medium was added to each small Petri dish (4 cm in diameter) containing the printed constructs.

Preparation of PNIPAM/nanocellulose-based stimuli-responsive bioink. The stimuli-responsive bioink was prepared using a formulation containing cellulose nanocrystals (CNC) from CelluForce (Canada), cellulose nanofibrils (CNF) provided by Empa (Switzerland), sodium alginate (SA), *N*-isopropylacrylamide (NIPAM), N,N′-methylenebisacrylamide (MBA) as crosslinker, and lithium phenyl-2,4,6-trimethylbenzoylphosphinate (LAP) as photoinitiator, following a previously reported protocol with minor modifications[30]. The nanocellulose-based bioink consists of 14 wt% CNC, 1 wt% CNF, 1.00 wt% of SA, 8.25 wt% of NIPAM, 0.06 wt% of MBA, 0.25 wt% LAP, and 75.44 wt% of deionized water. Briefly, CNC, SA, CNF suspension (at 2 wt%), NIPAM, and MBA were added in order, with thorough mixing using an overhead mechanical mixer after each addition until a homogeneous gel was obtained. LAP was added last, and all subsequent steps were performed under reduced light conditions to prevent premature photopolymerization. The formulation was mixed for an additional 3 min, transferred into printing syringes, protected from light with aluminium foil, and stored at 4 °C until use.

Bioprinting of artificial leaves. Two different types of artificial leaf-like structures were fabricated using direct ink writing (DIW) 3D printing technique (Allevi Inc., Philadelphia, PA, USA) of hydrogel formulations designed to reproduce plant-inspired geometries. Printing parameters were optimized according to the bioink formulation and the leaf size (1.5 or 3 cm in height). SA/HEC constructs were printed using a 27G plastic nozzle at a pressure of 70-75 kPa, a printing speed of 8

mm s^{-1}, and layer heights of 0.2 mm (1.5 cm leaves) or 0.5 mm (3 cm leaves).

PNIPAM/nanocellulose constructs were printed using a 25G stainless steel nozzle at a pressure of 45-50 kPa, a printing speed of 8.5 mm s^{-1}, and layer heights of 0.3 mm (1.5 cm leaves) or 0.4 mm (3 cm leaves). For both bioinks, a zigzag infill pattern with an infill distance of 0.5 mm and an infill direction of 0° was used. All samples were printed at room temperature (25 °C). The complete printing parameters are summarized in **Table 2**. Following the printing process, the PNIPAM/nanocellulose hydrogel constructs underwent UV crosslinking for the photopolymerization of PNIPAM, followed by an ionic crosslinking of SA, by immersing the structures in a 1 wt% calcium chloride ($CaCl_2$) aqueous solution for 24 h.

Tensile and bending characterizations. Mechanical characterization of the natural and artificial stem samples was performed using a custom-built mechanical testing system. Specifically, tensile and three-point bending tests were carried out using a micro-tensile stage equipped with a 10 N load cell (Honeywell, Charlotte, NC, USA) and driven by an electric stepper motor (Natech®, Munich, Germany; model ST4018M1804-KOWI1). The experimental setups for the tensile and three-point bending tests are shown in **Supplementary Figs. 6** and **9**, respectively.

For tensile testing, stem samples were mounted between two metal grips with an initial gauge length of 2-3.5 cm (i.e., 2 cm for artificial samples, 3.5 for natural samples) and subjected to uniaxial loading at a constant displacement rate of 0.2 mm s^{-1} until failure. Both natural and artificial stems were attached to the metal grips using a UV-curable adhesive (UHU Booster). For natural stems, tensile tests were performed on three stem regions corresponding to the basal, middle, and apical portions. Force and displacement were continuously recorded throughout the test.

Engineering strain (ε) was calculated as

$$\varepsilon = \Delta l / L$$

where:

- ε = engineering strain;

- Δl = displacement (mm);
- L = original length of the stem specimen (mm).

Engineering stress (**σ**) was calculated as

$$\sigma = F/A$$

where:

- σ = engineering stress (MPa);
- F = applied force (N);
- A = initial cross-sectional area (mm^2).

For solid cylindrical control samples, the cross-sectional area was calculated as

$$A = \pi * R^2$$

where:

- A = cross-sectional area (mm^2);
- π = mathematical constant (3.1416);
- R = cylinder radius (mm).

Natural and artificial stems exhibited a wheel-like cross-sectional architecture consisting of an outer ring and a central core separated by longitudinal air cavities. Therefore, the load-bearing cross-sectional area was approximated as the sum of the outer ring and the central cylindrical core according to:

$$A = A_{outer\ ring} + A_{central\ core} = \pi(R_o^2 - R_i^2) + \pi R_c^2$$

where:

- R_o =outer stem radius,
- R_i = inner radius of the outer ring (i.e., the radius enclosing the air lacunae),
- R_c= radius of the central core.

The structural Young's modulus in tension (**E_t, MPa**) was determined as the slope of the linear elastic region of the engineering stress-strain curve according to:

$\mathbf{E_t = \sigma / \varepsilon}$

The breaking stress and breaking strain were determined as the maximum engineering stress and strain recorded immediately before sample failure.

Three-point bending tests were performed using the same mechanical testing system equipped with a custom-made fixture and cylindrical indenter (Supplementary Fig. 9). Natural stem samples were positioned horizontally on two supports with a support span (*s*) of 3 cm, while a span of 2 cm was used for the artificial stems. A vertical load was applied at the midpoint of each specimen. For the natural stems, the mean span-to-diameter ratios were approximately 23:1, 20:1 and 28:1 for the basal, middle and apical regions, respectively. Owing to microfabrication constraints on the maximum achievable specimen length, a support span of 20 mm was used for the artificial stems. With a diameter of 2.7 mm, this corresponded to a span-to-diameter ratio of approximately 7.4:1. A vertical load was applied at the midpoint, and force and indenter displacement were continuously recorded throughout each test.

The flexural modulus (also known as Young's modulus in bending), ($E_{b,}$MPa) was then calculated as

$\mathbf{E_b = EI/I}$ where:

- (EI) is the flexural rigidity
- (I) is the second moment of area.

The bending stiffness (also known as flexural rigidity) (EI, $N \cdot mm^2$) was calculated as

$\mathbf{EI = s^3 * F/48\Delta}$

where:

- s= horizontal span of a stem (distance between clamps)
- F/Δ = the slope of the linear region of the force–deflection curve

For cylindrical control samples, the second moment of area (I) was calculated as

$I = \pi * R^4/4$ where (R) is the cylinder radius.

For natural and artificial stems, which exhibit a wheel-like cross-sectional architecture, the second moment of area was approximated as

$I = \pi(D_o^4 - D_i^4)/64 + \pi(D_c^4)/64$ where (D_o) is the outer stem diameter, (D_i) the inner diameter of the outer ring and (D_c) the diameter of the core.

All mechanical parameters were calculated from the linear elastic region of the corresponding force-displacement or stress-strain curves. Tensile tests on natural samples were performed with a sample size of n = 9, and bending tests with a sample size of n = 7. Tensional tests until failure on artificial samples were performed on a total of 8 bioinspired samples and 9 control samples. Only samples that failed at least 0.5 mm from the clamp were included in the analysis to minimize clamping artefacts, resulting in n=4 analyzed samples per group. Bending tests were performed on 6 bioinspired samples and 5 control samples. All results were analyzed in Prism 10 using an ANOVA with a Tukey HSD post-hoc test. Tests on natural samples were deemed sufficient for a first quantitative impression. All mechanical tests were performed at room temperature under ambient laboratory conditions.

Sensing characterizations. The environmental responsiveness of the PNIPAM/nanocellulose-based hydrogel leaves was evaluated by monitoring their deformation under changes in temperature (22-25° to approximatively 77°C) and salinity (0-6M NaCl). All experiments were performed in triplicate under aqueous conditions to mimic underwater environments. For temperature-response experiments, hydrogel leaves were initially immersed in deionized water at room temperature (22-25 °C), below the lower critical solution temperature (LCST) of PNIPAM (~32 °C). To induce hydrogel contraction, the samples were subsequently immersed in hot deionized water (~77 °C), above the PNIPAM LCST, prepared by heating the water in a microwave for 1 min. The samples were then returned to deionized water at room temperature, below the LCST, to evaluate the reversibility of the temperature-induced swelling-shrinking transition. Images were acquired throughout the heating and cooling cycles at regular time intervals.

For salinity-response experiments, hydrogel leaves were sequentially immersed in aqueous NaCl solutions with concentrations ranging from 0 to 6 M while maintaining identical experimental conditions. Structural deformation was recorded following each increase in salt concentration. For both temperature- and salinity-response experiments, images and videos were acquired using a digital camera positioned above the sample chamber. The projected surface area of the hydrogel leaves was quantified from the recorded image sequences using ImageJ (National Institutes of Health, Bethesda, MD, USA). Leaf bending was characterized by calculating the curvature of the leaf midline using the Kappa plugin for ImageJ. Curvature values were determined at each time point from the radius of curvature of the midline, enabling quantitative assessment of the reversible deformation and environmental sensing performance of the hydrogel leaves.

Artificial aquatic plant assembly and proof-of-concept experiments. Artificial stems and bioprinted leaves were assembled to fabricate fully integrated bioinspired aquatic plant-like machines. Leaves fabricated from either the SA/HEC microalgae-laden bioink or the stimuli-responsive PNIPAM/cellulose bioink were attached to the artificial stems at positions corresponding to the nodes of natural aquatic plants using a UV-curable adhesive (UHU Booster, UHU GmbH, Germany). After assembly, the artificial aquatic plants were immersed in water for all experiments. Proof-of-concept experiments were performed to demonstrate environmental sensing in underwater conditions. For temperature sensing, the assembled plants incorporating PNIPAM/cellulose leaves were exposed to controlled temperature changes using a laboratory hot plate. For salinity sensing, the plants were immersed in aqueous NaCl solutions of different concentrations. The deformation of the artificial leaves in response to the applied stimuli was recorded to evaluate the sensing capability of the biohybrid aquatic plants.

Author contributions

I.F. conceived and designed the study. I.F. performed the experiments, analyzed the data, and wrote the first draft of the manuscript. I.K. developed the protocol for the microalgae growth protocol and 3D printing. B.A. developed the bioink formulation for the stimuli-responsive artificial leaves. F.K.

contributed to the mechanical characterization and data analysis of the natural plant samples. B.M., T.S., and C.D. supervised the research. I.F., B.M., T.S., and C.D. acquired funding. All authors contributed to the interpretation of the results, revised the manuscript, and approved the final version.

Acknowledgements

I.F. was supported by a Fulbright Research Grant by US-Italy embassy to perform experiments at the California Institute of Technology from October 2023 to April 2024. I.F. was supported by a DAAD - Short-Term Research Grant for mobility by German Academic Exchange Service to perform experiments at the University of Freiburg from May to July 2022. T.S. and I.F. acknowledges funding by by the Deutsche Forschungsgemeinschaft (DFG, German Research Foundation) under Germany's Excellence Strategy-EXC-2193/1-390951807 and access to the shared laboratory facilities of the cluster. We thank Madeleine Tomasovic Savigny from Cellink company for technical support with the LumenX bioprinter. We would like to thanks Jessika Huss and Sebastian J. Antreich from Institute of Biophysics (University of Natural Resources and Life Sciences (BOKU), 1190 Vienna, Austria) for providing the dry samples of *Trapa natans* fruits. We thank Michael Schmidt for support with histology work. I.K. and C.D. acknowledge the NSF for their financial support through the Grant No. 2308575. This work was supported by the Resnick Sustainability Institute at Caltech. The authors thank Dr. Nate Glasser for performing confocal microscopy analysis using instrumentation in the Resnick Ecology and Biosphere Engineering Facility. I.K. acknowledges Fulbright Israel for the financial support.

Conflict of interest

Authors have no competing interests.

Supplementary information

Supplementary Information is available for this paper.

Data availability

The manuscript, Supplementary Information, and Supplementary Movies contain all data necessary

to evaluate the conclusions of this study. The supporting materials are also available in Figshare at https://doi.org/10.6084/m9.figshare.34655367. The raw data generated and analysed during the current study are available from the corresponding author, Isabella Fiorello.

Figures

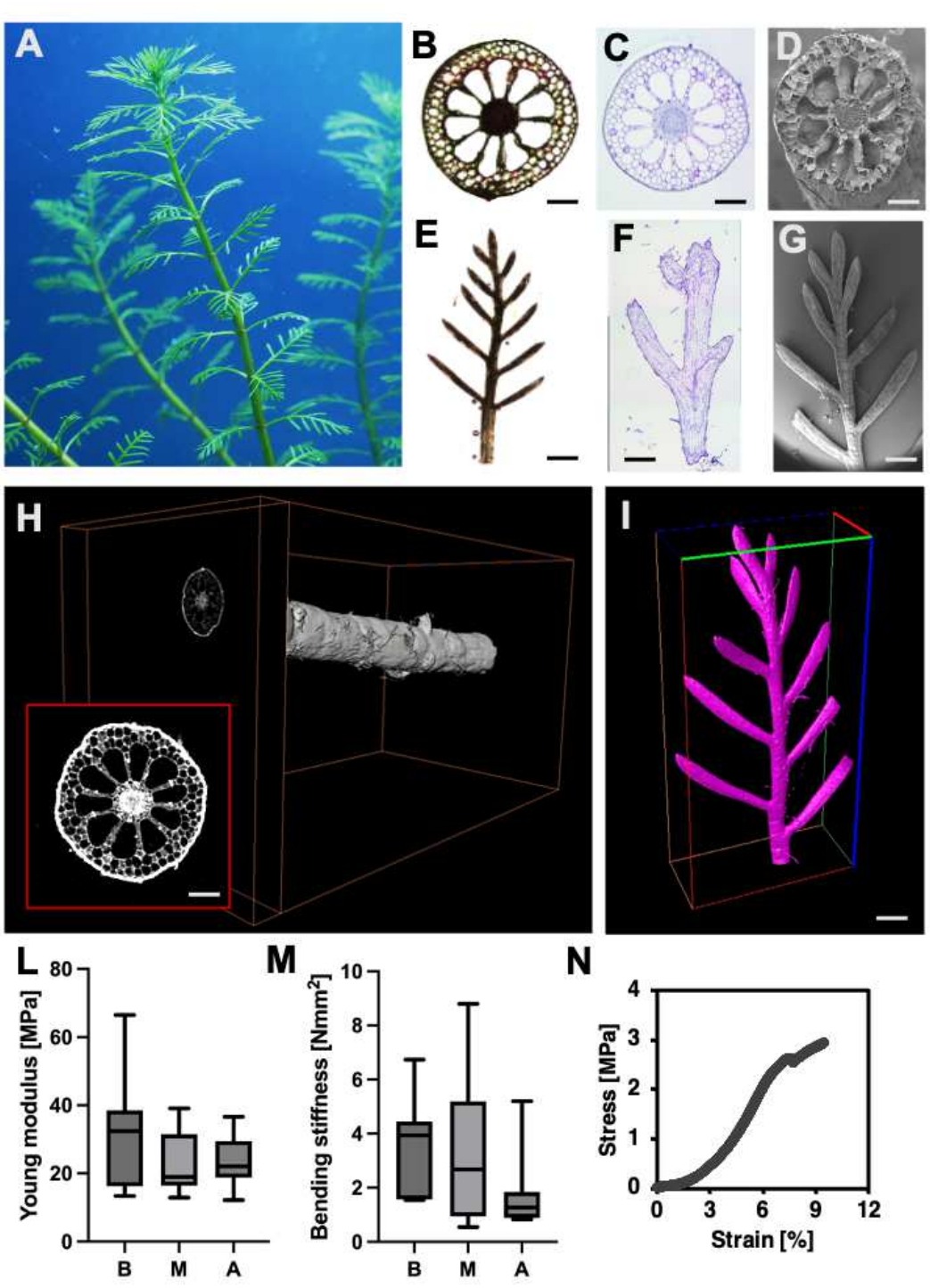


Fig. 1. Bioinspiration from aquatic plants for bioinspired soft machines. (A) Representative

submerged aquatic plant (*Myriophyllum mattogrossense*) in an aquarium. (B-G) Optical, histological, and electron microscopy images of *Myriophyllum* stems and leaves. (H, I) Cross-sectional imaging and three-dimensional micro-computed tomography of stem and leaves. (L) Structural Young's modulus measured in tension for basal (B), middle (M) and apical (A) stem regions. (M) Bending stiffness of basal, middle and apical stem regions. (N) Representative tensile stress–strain curve of a *M. mattogrossense* stem sample. Scale bars: (B-D) 500 µm; (E-G) 1 mm; (H, inset) 500 µm; (I) 1 mm.

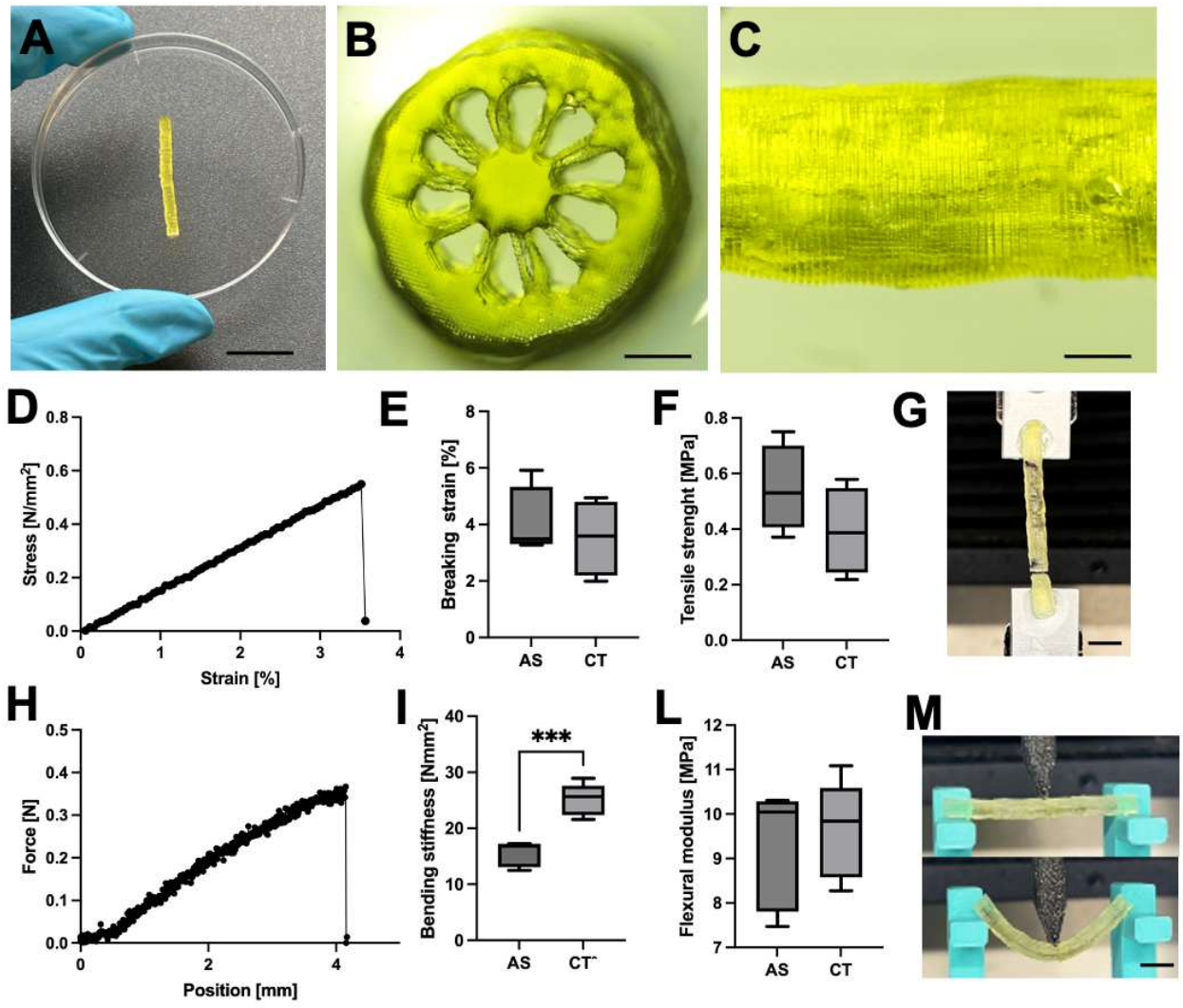


Fig. 2. Bioprinted aquatic plant-inspired stems and mechanical characterization. (A) Bioprinted artificial stem inspired by the internal architecture of aquatic plant stems. (B, C) Optical images of cross-sectional (B) and longitudinal (C) views of the bioprinted stem,

revealing plant-inspired internal porosity and aligned structures. (D) Representative stress–strain response under uniaxial tensile loading. (E, F) Comparison of breaking strain (E) and tensile strength (F) between artificial stems (AS) and control samples (CT). (G) Experimental setup for tensile testing. (h) Representative force–displacement response during three-point bending tests. (I, L) Comparison of bending stiffness (I) and structural Youngs modulus (L) between artificial stems (AS) and control samples (CT). (m) Three-point bending test showing large, reversible deformation of the bioprinted stem. Scale bars: (A) 1 cm; (B, C) 1 mm; (G, M) 5 mm.

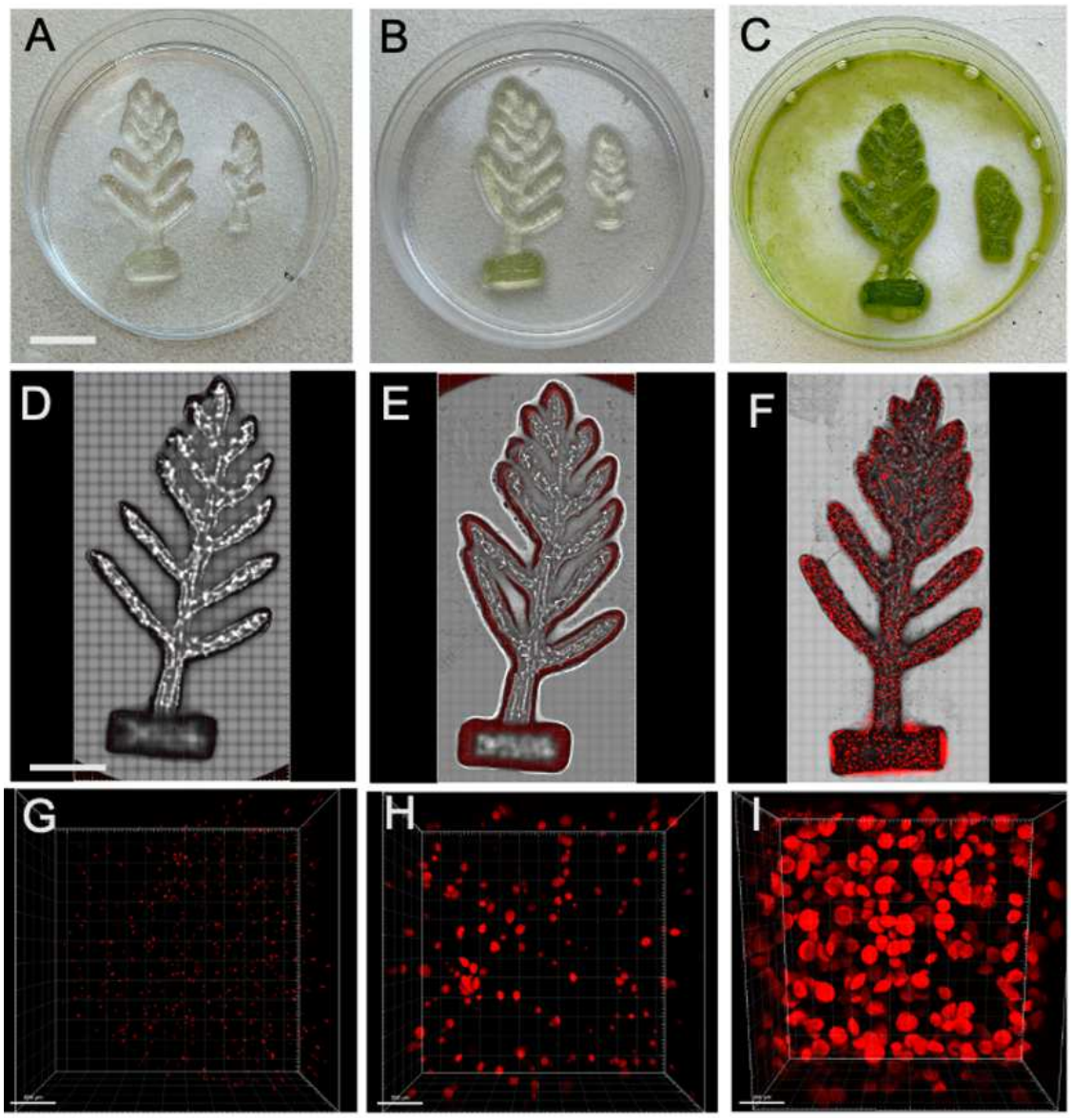


Fig. 3. Bioprinted leaf-like sodium alginate-hydroxyethyl cellulose hydrogels with embedded microalgae. (A-C) Optical images of bioprinted plant-inspired hydrogel structures containing *Chlamydomonas reinadii* algae at day 0 (A), intermediate culture (B), and day 21 (C), showing the transition from transparent to green as a result of algal growth. (D-F) Confocal microscopy images of the hydrogel structures (G-I) Three-dimensional confocal microscopy reconstructions showing the spatial distribution and increased density of viable microalgae within the hydrogel matrix over time. Scale bars: (A) 0.5 cm; (D-F) 0.25 cm; (G-I) 50 µm.

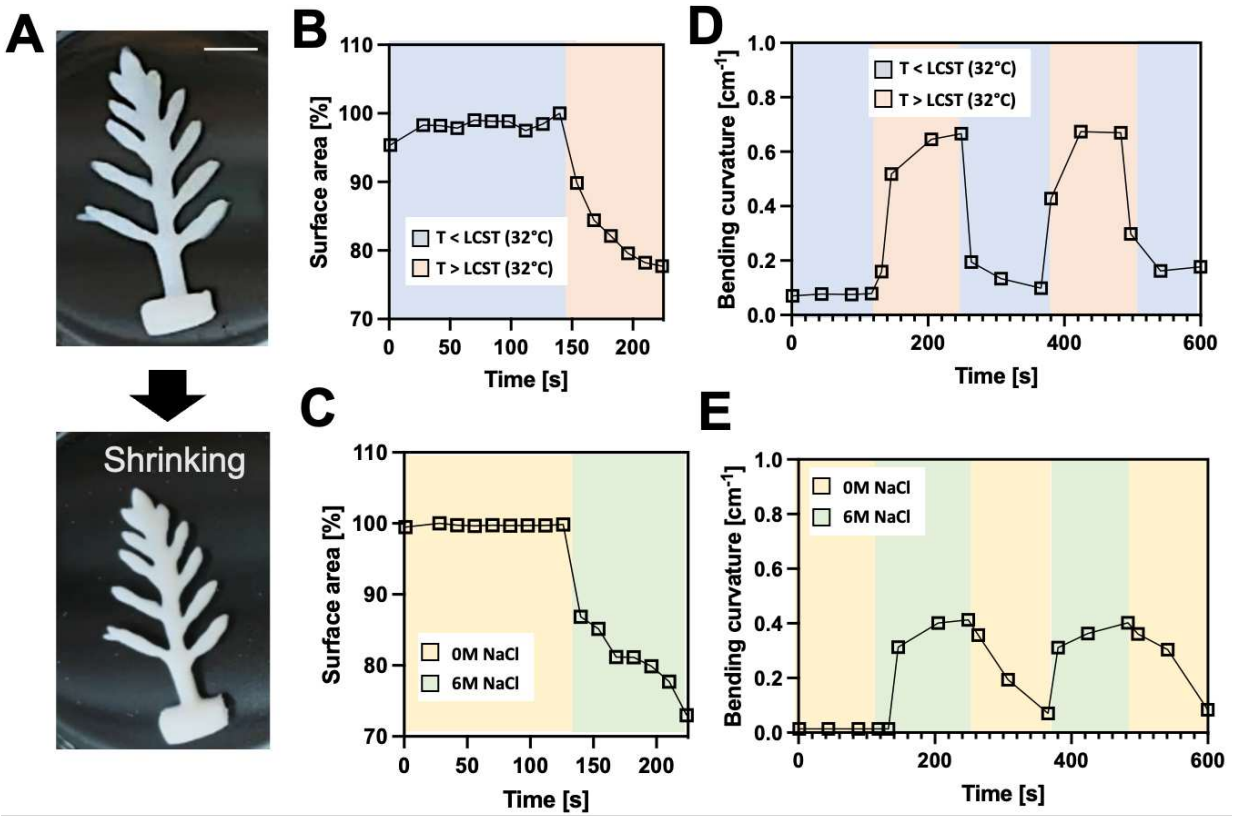


Fig. 4. Bioprinted leaf-like PNIPAM/nanocellulose-based hydrogels for underwater sensing. (A) Bioprinted plant-inspired structure fabricated from PNIPAM/nanocellulose-based hydrogel, showing reversible shrinking in response to external stimuli. Scale bar: (A) 0.75 cm. (B, C) Time evolution of surface area in response to temperature changes across PNIPAM's lower critical solution temperature (LCST, 32 °C) (B) and to salinity variations (0-6 M NaCl) (C). (D, E) Corresponding bending curvature as a function of time under cyclic temperature (D) and salinity

(E) stimuli, demonstrating reversible swelling shrinking behavior and sensing capability in aquatic environments.

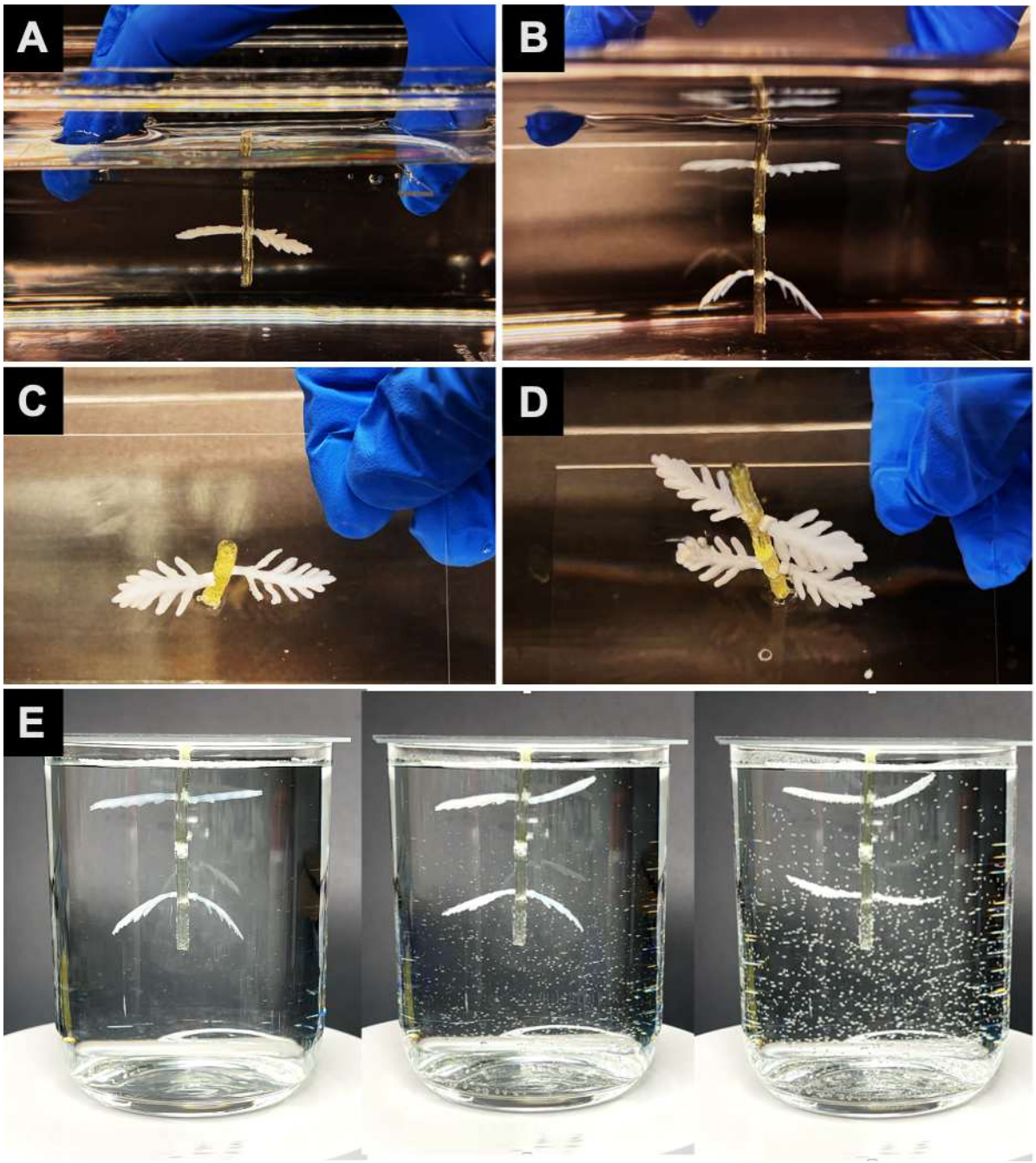


Fig. 5. Integrated aquatic plant-like machine for underwater operation. (A, B) Assembly of the bioprinted artificial stem and leaves to form an integrated aquatic plant-like soft machine. (C, D) Handling and manipulation of the integrated structure, showing mechanical robustness and compliance in water. (E) Proof-of-concept demonstration of the artificial aquatic plant operating

underwater, exhibiting passive reconfiguration and deformation in response to environmental conditions (from room temperature to boiled water after 15 to 30 minutes, from left to right), highlighting its potential for underwater sensing applications.

References

1 Wang, J., Soininen, J. & Heino, J. Vol. 132 108250 (Elsevier, 2021).

2 Li, G. *et al.* Bioinspired soft robots for deep-sea exploration. *Nature Communications* **14**, 7097 (2023). https://doi.org:10.1038/s41467-023-42882-3

3 Mazzolai, B. & Laschi, C. A vision for future bioinspired and biohybrid robots. *Science robotics* **5**, eaba6893 (2020).

4 Kim, S., Laschi, C. & Trimmer, B. Soft robotics: a bioinspired evolution in robotics. *Trends in biotechnology* **31**, 287-294 (2013).

5 Prescott, T. J. & Verschure, P. F. Living machines: An introduction. *Living machines: A handbook of research in biomimetics and biohybrid systems*, 1 (2018).

6 Bar-Cohen, Y. & Breazeal, C. Biologically inspired intelligent robots. *Smart Structures and Materials 2003: Electroactive Polymer Actuators and Devices (EAPAD)* **5051**, 14-20 (2003).

7 Ilami, M., Bagheri, H., Ahmed, R., Skowronek, E. O. & Marvi, H. Materials, actuators, and sensors for soft bioinspired robots. *Advanced Materials* **33**, 2003139 (2021).

8 Xia, Z. *Biomimetic Principles and Design of Advanced Engineering Materials*. (John Wiley & Sons, 2016).

9 Mazzolai, B., Beccai, L. & Mattoli, V. Plants as model in biomimetics and biorobotics: new perspectives. *Frontiers in bioengineering and biotechnology* **2**, 2 (2014).

10 Fiorello, I., Del Dottore, E., Tramacere, F. & Mazzolai, B. Taking inspiration from climbing plants: Methodologies and benchmarks–A review. *Bioinspiration & Biomimetics* (2020).

11 Mazzolai, B., Tramacere, F., Fiorello, I. & Margheri, L. The bio-engineering approach for plant investigations and growing robots. A mini-review. *Frontiers in Robotics and AI* **7** (2020).

12 Speck, T. *et al.* Plants as inspiration for material-based sensing and actuation in soft robots and machines. *MRS Bulletin*, 1-16 (2023).

13 Hawkes, E. W., Blumenschein, L. H., Greer, J. D. & Okamura, A. M. A soft robot that navigates its environment through growth. *Science Robotics* **2**, eaan3028 (2017).

14 Sadeghi, A., Mondini, A. & Mazzolai, B. Toward self-growing soft robots inspired by plant roots and based on additive manufacturing technologies. *Soft robotics* **4**, 211-223 (2017).

15 Coad, M. M. *et al.* Vine robots: Design, teleoperation, and deployment for navigation and exploration. *arXiv preprint arXiv:1903.00069* (2019).

16 Fiorello, I., Mondini, A. & Mazzolai, B. in *2023 IEEE International Conference on Soft Robotics (RoboSoft).* 1-7 (IEEE).

17 Fiorello, I. *et al.* Climbing Plant-Inspired Micropatterned Devices for Reversible Attachment. *Advanced Functional Materials* **30**, 2003380 (2020).

18 Fiorello, I., Ronzan, M., Speck, T., Sinibaldi, E. & Mazzolai, B. A Biohybrid Self-Dispersing Miniature Machine Using Wild Oat Fruit Awns for Reforestation and Precision Agriculture. *Advanced Materials*, 2313906 (2024).

19 Fiorello, I. *et al.* Plant-like hooked miniature machines for on-leaf sensing and delivery. *Communications Materials* **2**, 1-11 (2021).

20 Fiorello, I., Meder, F., Tricinci, O., Filippeschi, C. & Mazzolai, B. in *Conference on Biomimetic and Biohybrid Systems.* 122-133 (Springer).

21 Miler, O., Albayrak, I., Nikora, V. & O'Hare, M. Biomechanical properties of aquatic plants and their effects on plant–flow interactions in streams and rivers. *Aquatic Sciences* **74**, 31-44 (2012).

22 Garmroudi, A., Tushar, M. A. K., Liu, C. & Li, Z. Biohybrid living robotics: A comprehensive review of recent advances, technological innovation, and future prospects. *npj Robotics* **3**, 43 (2025).

23 Mainik, P., Spiegel, C. A. & Blasco, E. Recent advances in multi-photon 3D laser printing: active materials and applications. *Advanced Materials* **36**, 2310100 (2024).

24 Zhang, Y. S. *et al.* 3D extrusion bioprinting. *Nature Reviews Methods Primers* **1**, 75 (2021). https://doi.org:10.1038/s43586-021-00073-8

25 Guida, L., Cavallaro, M. & Levi, M. Advancements in high-resolution 3D bioprinting: Exploring technological trends, bioinks and achieved resolutions. *Bioprinting* **44**, e00376 (2024). https://doi.org:https://doi.org/10.1016/j.bprint.2024.e00376

26 Fiorello, I., Liu, Y., Kamare, B. & Meder, F. Harnessing chemistry for plant-like machines: from soft robotics to energy harvesting in the phytosphere. *Chemical Communications* **61**, 6246-6259 (2025).

27 Ferro, Y., Perullini, M., Jobbagy, M., Bilmes, S. A. & Durrieu, C. Development of a biosensor for environmental monitoring based on microalgae immobilized in silica hydrogels. *Sensors* **12**, 16879-16891 (2012).

28 Boons, R. *et al.* Light-based 3D printing of mechanoluminescent living gels loaded with dinoflagellates. *Science Advances* **12**, eadz0017 (2026). https://doi.org:doi:10.1126/sciadv.adz0017

29 Arsuffi, B., Magrini, T., Champeau, M., Siqueira, G. & Titotto, S. 4D printing of natural materials: A review. *Sustainable Materials and Technologies* **44**, e01346 (2025). https://doi.org:https://doi.org/10.1016/j.susmat.2025.e01346

30 Arsuffi, B. *et al.* Programmable multi-responsive nanocellulose-based hydrogels with embodied logic. *Advanced Functional Materials* **34**, 2409864 (2024).

Supplementary Files

This is a list of supplementary files associated with this preprint. Click to download.

- MovieS5.mp4
- MovieS6.mp4
- MovieS10.mp4
- MovieS20.mp4
- MovieS12.mp4
- MovieS13.mov
- MovieS11.mp4
- MovieS17.mp4
- MovieS4.mov
- MovieS8.mp4
- MovieS18.mp4
- MovieS9.mov
- MovieS15.mp4
- MovieS3.mp4
- MovieS19.mp4
- MovieS14.mov
- MovieS16.mp4
- MovieS2.mp4
- MovieS1.mov
- SupplementaryInformation.pdf
- MovieS7.mp4